ENVIRONMENTAL RESEARCH COMMUNICATIONS

INCLUSIVE PUBLISHING TRUSTED SCIENCE

ACCEPTED MANUSCRIPT • OPEN ACCESS

Ozone Production over Arid Regions: Insights into Meteorological and Chemical Drivers

To cite this article before publication: Mohammad Amin Mirrezaei *et al* 2024 *Environ. Res. Commun.* in press https://doi.org/10.1088/2515-7620/ad484c

IOP Publishing *Environmental Research Communications*

Ozone Production over Arid Regions: Insights into Meteorological and Chemical Drivers

Mohammad Amin Mirrezaei[1*], Avelino Arellano[1,2], Yafang Guo[1], Chayan Roychoudhury[1] and Armin Sorooshian[1,2]

[1] Department of Hydrology and Atmospheric Sciences, University of Arizona, Tucson, AZ, USA

[2] Department of Chemical and Environmental Engineering, University of Arizona, Tucson, AZ, USA

E-mail: amirrezaei@arizona.edu

Abstract

Arid urban areas are pivotal in the global landscape, and their air quality issues are highlighted by the complexities of tropospheric ozone production. Here, we use recent satellite observations from TROPOMI and a longer record of data from OMI to investigate the levels of ozone precursors (NO_2 and CH_2O) in 12 major cities in arid regions. Using a space-based CH_2O/NO_2 indicator, we identified the dominant chemical regime influencing ozone formation, revealing a clear temporal trend that aligns with previously reported economic trajectories as well as variation in emission control strategies implemented in these cities. Our results show that, NO_2 concentrations decreased in cities with proactive regulatory policies, such as Madrid and Los Angeles in semi-arid and arid regions. A contrasting increase was observed in rapidly developing cities within arid and hyper-arid regions, such as Tehran and Cairo, where emission controls are less strict. An increase in CH_2O levels was also apparent, requiring more attention to VOCs control. Furthermore, our analysis clearly shows that the interactions between ozone production and climatic factors such as temperature exhibit a nonlinear relationship, especially in arid climates. These findings highlight the importance of emission reduction strategies that consider the meteorological and chemical drivers of dry regions, particularly in light of the rising global aridity.

Keywords: Ozone Precursors, Aridity, TROPOMI, OMI, O_3, Tropospheric Ozone Production

1. Introduction

According to the Intergovernmental Panel on Climate Change (IPCC), urban areas are particularly vulnerable to the effects of climate change [1, 2]. Urban migration has significantly increased in recent decades. Globally, 1692 urban areas are classified as "Big Cities" which have a population of more than 300,000 [2]. Climate change has had a significant impact on aridity in urban areas. The aridity index (AI) is a commonly used method for determining the level of aridity and its variations. According to the UNEP (United Nations Environment Programme) classification [3], the AI is classified as hyper-arid (<0.03), arid (0.03 - 0.2), semi-arid (0.2 – 0.5), dry sub-humid (0.5 – 0.65), and humid (>0.65). It is calculated by dividing the amount of precipitation by the potential evapotranspiration (PET) [4]. Based on the classification provided, it was observed that 35% (586) out of the total 1692 big cities fall within dryland areas, where the AI is equal to or less than 0.65 [2]. Cities in arid regions have diverse geographical

distributions and populations. According to the United Nations' classification of global cities, four out of the ten most populous cities in 2018, namely Delhi, Beijing, Cairo, and Mexico City, are located in drylands [5]. Furthermore, a significant proportion of the major urban centers in arid regions are in developing countries such as Kuwait, Baghdad, Riyadh, and Khartoum. These cities are characterized by the highest rates of urban population growth [6]. Moreover, multiple studies have revealed that if moderate measures are taken to reduce greenhouse gas emissions, with the assumption that global annual emissions will reach their highest point around 2040 and then decrease (RCP 4.5), and also in the highest baseline emissions scenarios with no significant efforts to mitigate emissions (RCP 8.5), a significant proportion of non-dryland cities will experience increased aridity in the future [2, 4, 7-10].

Another key factor to consider in these areas is the susceptibility to air pollution. This susceptibility arises from a combination of factors, including the presence of diverse and significant emissions from both human activities (anthropogenic) and natural sources (biogenic), as well as greater vulnerability to the effects of climate change [11]. Drought and higher temperatures can contribute to elevated levels of air pollution, particularly an increase in ozone concentrations, through the acceleration of photochemical reactions [12-14]. *Figure 1* shows the spatial distribution of extreme surface ozone concentrations from 2005 to 2022 using CAMS reanalysis data. It highlights areas where the average 90th percentile of the 3h surface ozone is particularly high. These high ozone areas are not uniformly spread but are notably prevalent in cities located in dryland regions, which include hyper-arid (marked in beige), arid (brown), and semi-arid (green) zones. Except for major cities in China, North America, India, and Europe, limited research on ozone pollution has been conducted in dryland cities.

Tropospheric ozone production is a nonlinear and complex process that is influenced by a number of factors, including the emission of precursors, mainly nitrogen oxides (NO_x) and volatile organic compounds (VOCs), and meteorological parameters such as temperature, solar radiation, and relative humidity, and transport [15-20]. Several previous studies have examined the relationship between meteorological parameters and O_3 production. They demonstrated that elevated temperatures enhance photochemical reactivity, which increases the rate of O_3 generation while altering emissions from natural precursors [21-23]. Furthermore, elevated humidity levels have the potential to enhance the presence of clouds and act as a proxy for HO_x (OH (hydroxyl) + HO_2 (peroxyl)) concentration, which may result in a reduction in the efficiency of photochemical reactions associated with O_3 [21, 24, 25]. In addition to meteorology, precursor (NO_x and VOCs) levels also affect ozone production. According to [26], ambient ozone production is primarily influenced by either NO_x (NO_x-limited regime) or volatile organic compounds (VOCs, VOC-limited regime). Thus, the utilization of an optimal VOCs/NO_x ratio can thus serve as an indicative measure for distinguishing between the NO_x-limited and VOC-limited regimes. Accurately identifying the chemistry of O_3 is critical for developing effective measures for reducing O_3 pollution. The present methods utilized for determining the sensitivity of O_3-NO_x-VOCs include observation-based methods, satellite retrievals, and model approaches. Ground-based networks across the globe lack the necessary resolution and coverage to assess spatially representative trends accurately. Additionally, the lack of modeling infrastructure exacerbates this limitation. Satellite-derived measurements of formaldehyde (CH_2O) and nitrogen dioxide (NO_2) column densities have been widely used to investigate regional and temporal variations in VOCs and NO_x emission rates, respectively. The utilization of satellite indicators entails inherent uncertainties, such as errors in satellite retrievals, lack of vertically resolved data, and lack of establishment of thresholds for NO_x/VOC-limited regimes [27-30].

The effectiveness of tropospheric columnar CH_2O/NO_2 (formaldehyde-to-nitrogen dioxide ratio or FNR) values in indicating local ozone production is limited by the variability in the CH_2O and NO_2 levels.

[27] found that the largest errors in this ratio stem from uncertainties in satellite derived CH_2O levels for the tropospheric column, which exceed the errors for NO_2. Furthermore, the accuracy of the ratio was compromised by the uncertain correlations between columnar CH_2O and surface-level organic reactivity.

[31] and [32] used the Global Ozone Monitoring Experiment (GOME) and Ozone Monitoring Instrument (OMI) satellite sensors, respectively, to determine the NO_x-limited and VOC-limited ozone formation regimes based on thresholds defined using the GEOS-Chem and CMAQ models. A recent study [33] presented a more precise approach to utilizing the FNR from OMI as an indicator of surface ozone production based on thresholds defined using surface measurements. The assessment of 1) dominant chemical regimes and 2) the relative impact of meteorological and chemical precursors on ozone production in cities within dry areas is limited, as previous studies were conducted on different timescales and with different indicators.

Here, we investigate for the first time the patterns of CH_2O, NO_2, and associated FNR over 12 cities in semi-arid, arid, and hyper-arid regions with varying levels of emissions and population using the Tropospheric Monitoring Instrument (TROPOMI) and OMI tropospheric formaldehyde (CH_2O) and NO_2 columns to elucidate ozone production chemical regimes during recent years (2005–2022). In particular, we aim to: 1) provide a classification of current arid cities based on the most recent and widely used aridity index to explore the evolution of ozone production chemical regime in each aridity category; 2) compare cities in each category and different categories based on their population, and dominant source characteristics; 3) investigate the change in ozone production regimes during the COVID-19 lockdown; and 4) unravel the relative dependence of the chemical regime of cities in each aridity class on temperature and relative humidity and provide a picture of the possible characteristics of the ozone production regime for future climate.

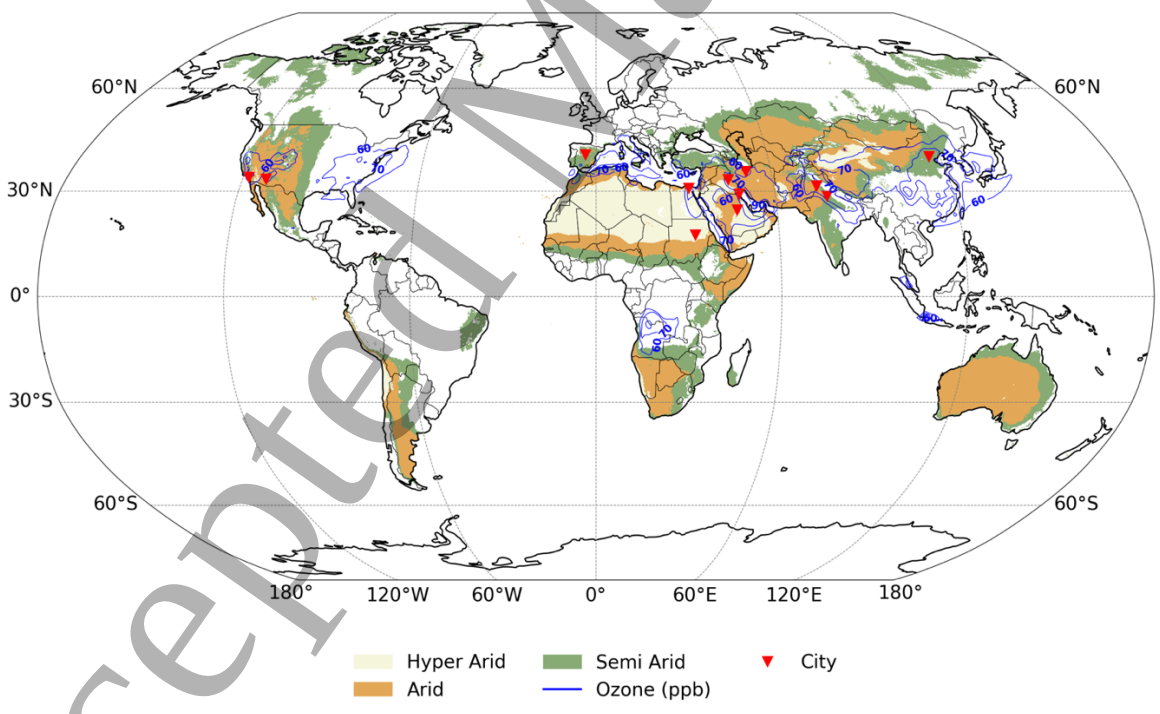

Figure 1. **Semi-arid (green), arid (brown), and hyper-arid (beige) regions superimposed on 90th percentile of 3h CAMS reanalysis surface ozone contours (blue contours). The location of 12 cities examined in this work are shown as red markers.**

2. Materials and Methods

2.1 Study area

To identify urban areas situated in dry regions characterized by semi-arid, arid, and hyper-arid climates, we employed the Global Aridity Index and Potential Evapotranspiration Database, Version 3, which was published in 2022 [4]. The data were geographically aligned with the shapefile of each city and the median value of the aridity index was used to depict the level of aridity in each respective city. In order to diversify the choice of cities across population counts and different continents, we chose the following cities (shown in *Figure 1*) listed in order of ascending population counts: Madrid (Spain), Lahore (Pakistan), Beijing (China), and Delhi (India) for semi-arid cities; Phoenix (USA), Los Angeles (USA), Baghdad (Iraq), and Tehran (Iran) for arid cities; and Khartoum (Sudan), Kuwait City (Kuwait), Riyadh (Saudi Arabia) and Cairo (Egypt) for hyper-arid cities. To consider the populated and polluted parts of each city, world urban shapefiles from the Esri Maps and Data group [34] were used to mask data over city areas. The distribution of the aridity index over each city's shapefile is shown in *Figure S1*. To further investigate the characteristics of the cities in different dry climates, a 100-m-resolution global map of local climate zones (LCZs), composed of 10 built and seven natural land cover types that capture the character of the urban landscape, was also masked to the shapefile of each city [35]. *Figure S2* shows the seven natural land cover types in cities with different aridity categories. Defining a shapefile that is representative of a city is critical for an accurate representation of tropospheric NO_2 and CH_2O columns, aridity index, local climate zones, and meteorological factors such as temperature and relative humidity.

To represent the ozone production chemical regime in the selected cities, daily FNR tropospheric columns for the OMI instrument were calculated for all pixels inside the shapefile of each city from 2005 to 2020. In addition, to demonstrate the more recent and higher-resolution FNR over cities, the daily FNR from TROPOMI CH_2O and NO_2 tropospheric columns were also calculated. To define NO_x- or VOC-limited regimes, [33] recommended thresholds that we used (<3.2 VOC-limited, 3.2-4.1 transition, and >4.2 NO_x-limited), as successfully demonstrated in recent studies showing acceptable agreement with chemical regimes defined by surface measurements [36, 37]. The use of a constant threshold for satellite-based ozone formation mechanisms across various regions of the world may increase uncertainty. Owing to the lack of long-term records of ozone concentration in dry cities, particularly those in Asia and Africa, the same approach as [33] to calculate local thresholds is not applicable to these regions, which can be considered a limitation of the present study.

2.2 Satellite Data

2.2.1 TROPOMI

This study utilized TROPOMI Level 2 data, specifically the tropospheric column observations of NO_2 and CH_2O version 2, obtained from the NASA Goddard Earth Sciences Data and Information Services Centre. These data were used to examine the temporal and spatial variations in ozone precursors. TROPOMI is a spectrometer that operates in the ultraviolet, visible, near-infrared and shortwave ranges. It is installed on the S5P satellite and the spatial resolution of TROPOMI is approximately 5.5×3.5 km^2 at nadir [38, 39]. The data utilized in this research underwent a quality control process, where a quality assurance value (qa_value) greater than 0.50 was applied for CH_2O and a qa_value greater than 0.75 was applied for NO_2 [40, 41]. The dataset was gridded to a resolution of 0.07°×0.07° to facilitate further analyses.

2.2.2 OMI

Tropospheric NO_2 and CH_2O retrievals were obtained from the OMI from 2005 to 2020 to examine the decadal trend of the FNR across selected cities. OMI is a sensor designed to detect atmospheric composition by measuring backscattering solar radiation across the spectral range of 270–500 nm [42, 43]. Similar to TROPOMI, OMI exhibits a passing time of around 13:45 local time. In this study, Level-3 daily global gridded (0.25° × 0.25°) tropospheric NO_2 vertical column density (VCD) data are used from the version 4 release, which has undergone improvements by the integration of refined air mass factors (AMFs) [44]. Furthermore, we employed tropospheric CH_2O vertical columns that were developed under the QA4ECV[1] project [45, 46]. In this study, we employed level 2 data and regridded data to a spatial resolution of 0.25° by 0.25°, using area-weighted averaging of the finer pixels.

2.2.3 ERA-5 and CAMS Reanalysis

In this study, we used hourly atmospheric and dew point temperature at 2 m from ERA5 reanalysis, which refers to the fifth generation of the European Center for Medium-Range Weather Forecasts (ECMWF) global reanalysis with a spatial resolution of 0.25° × 0.25° from 2019 to 2022 [47]. Due to the limitations of the ERA5 dataset where hourly relative humidity in the single level dataset is not available, the relative humidity (RH) was calculated based on the empirical Magnus formula using the ratio of the actual vapor pressure to the saturation vapor pressure [48]. In order to maintain consistency with satellite retrievals, the temperature and dew point (to calculate relative humidity) data were averaged over the duration of satellite overpasses for each city. Furthermore, we utilized the 3-hourly surface ozone data from the CAMS reanalysis dataset, which is the most recent global reanalysis dataset of atmospheric composition (AC) generated by the Copernicus Atmosphere Monitoring Service (CAMS) [49]. The dataset has a spatial resolution of approximately 80 km. Our objective was to construct a global spatial map of surface ozone extremes (i.e., the mean of the 90th percentile), spanning from 2005 to 2022.

2.2.4 Aridity Index

AI is a metric that quantifies the balance between precipitation and potential evapotranspiration (*PET*), which reflects the atmospheric demand for water. It is conventionally calculated as the ratio of the mean annual precipitation (MA_{Prec}) to the mean annual reference evapotranspiration (MA_{ET0}). This index is a measure of the volume of incoming precipitation with the potential volume of water that could be lost to the atmosphere, thereby indicating the amount of moisture potentially available for use by plants and in the soil. The formula for the aridity index is given as:

$$\mathrm{AI} = \frac{\mathrm{MA_{Prec}}}{\mathrm{MA_{ET0}}}$$

where AI is the Aridity Index, MA_{Prec} is the Mean Annual Precipitation, and MA_{ET0} is the Mean Annual Reference Evapotranspiration. We used the Global Aridity Index and Potential Evapotranspiration Database, Version 3, which provides 30 arc-second spatial resolution with monthly and yearly averages for the period from 1970 to 2000 [4].

[1] Quality Assurance for Essential Climate Variables

2.2.5 Mutual Information

In our analysis, we utilized the *mutual_info_regression* function from the scikit-learn library for feature selection to help us choose which features/predictors are important when predicting a target. Mutual information (MI) is a measure of the nonlinear dependency between variables, capturing relationships that may not be apparent through linear correlation alone. An added advantage is that we can calculate this dependency without assuming a specific relationship between the predictors and the target [50, 51]. The MI metric is based on the joint probability distribution density between the feature and the target based on entropy estimates from k-nearest neighbor distances. The details of the algorithm are outlined in [52]. An MI value of 0 suggests that the predictor and the target are independent, while higher values mean higher dependency. The values are measures of "amount of information" in *bits*, based on information theory [53].

3. Results and Discussions

3.1 Analysis of FNR over different cities

Figure 2 illustrates the temporal evolution of the FNR from 2005 to 2020 across cities in semi-arid, arid, and hyper-arid regions. Cities are organized in rows from left to right, in ascending order of population size.

- Semi-arid Cities:

The temporal trend in the FNR for semi-arid cities indicates an overall increase, with Lahore being an exception. As shown in *Table S1,* Madrid and Beijing experienced the most notable increases with the average rises of 87.32% and 57.14% during the period 2017-2020 compared to 2005-2008, while Delhi's increase was comparatively smaller (22.68%). *Figures S3—S6* and *Tables S1-S3* show that this trend was primarily due to a decrease in NO_2 values, particularly in Madrid and Beijing (43.91% and 40.41% decreases during the period 2017-2020 relative to 2005-2008). In contrast, the CH_2O column remained relatively stable or increased slightly compared to the changes in NO_2 levels, resulting in an increasing in FNR over time (*Figures S3-S6* and *Tables S1-S3*). This finding is consistent with previous studies as OMI NO_2 levels dropped significantly in Madrid between 2005 and 2014, with a 45-55% decrease in Barcelona [54]. Other studies reported NO_2 reductions from 2005 to 2019 in Beijing and Delhi [54-56]. Conversely, Lahore experienced an increase in NO_2 [54, 56]. *Figure S5* shows that OMI NO_2 levels followed similar trends in these cities. Looking at the global CAMS-ANTv5.3 [57] monthly averaged anthropogenic NO_2 emissions from 2005 to 2019 (*Figures S7* and *S8*), except for Beijing, OMI NO_2 levels indicate a reduction in NO_2 emissions. The overestimation of NO_2 emissions in CAMS global anthropogenic emissions has also been reported as a positive bias of NO_2 surface concentration from CAMS reanalysis over China [58]. The difference between emissions and observations can be explained by China's 2018–2020 Clean Air Plan (CAP), which was reported to be effective [58]. In terms of the ozone production chemical regime, an increase in FNR causes the chemical regime in Madrid to shift from VOC-limited to transitional regime between May and August. A similar pattern was observed in Delhi. In Lahore, a reverse pattern was observed, with the chemical regime shifting from near NO_x-limited during the summer to near VOC-limited. In Beijing, as NO_2 levels decreased, the chemical regime shifted to a higher FNR and was closer to the transition regime. Cities in semi-arid regions experienced a VOC-limited regime throughout the winter, which is primarily due to higher NO_2 and lower CH_2O levels during this season.

- Arid Cities:

Among arid regions, Phoenix and Los Angeles followed the trends observed in Madrid, Beijing, and Delhi (semi-arid), with the average 48.63% and 57.39% reductions in their NO_2 tropospheric column, respectively, during 2017-2020 compared to 2005-2008. Conversely, Tehran and Baghdad experienced increases in NO_2 levels over the same periods, at 37.94% and 9.42%, respectively. This is reflected in the NO_2 trends (*Figures S3*, *S5 and tables S1* and *S3*), which decrease in the former cities and increase in the latter. Previous studies have highlighted the significant NO_2 reduction in Los Angeles [59], whereas increasing NO_2 levels by Baghdad and Tehran have been reported [54, 56]. Unlike other cities, Los Angeles, and Phoenix, experienced a decrease in CH_2O levels (6.27% and 3.89% reduction, respectively, during the period 2017-2020 relative to 2005-2008). However, the rate of decrease of NO_2 was greater than that of CH_2O, resulting in higher FNRs values over time. Changes in the FNR resulted in changes among the chemical regimes in these cities. In all cities, winter remained in a VOC-limited regime, but during summer, Phoenix's chemical regime has shifted from VOC-limited/transition to nearly NO_x-limited in recent years. Los Angeles followed a similar trend, changing from a VOC-limited regime in the summer of 2005-2008 to a transitional regime in 2017-2020. For Baghdad and Tehran, an increase in both NO_2 and CH_2O maintained a VOC-limited regime throughout the year.

- Hyper-arid Cities:

Except for Riyadh and Kuwait, the hyper-arid cities remained relatively stable over time, with consistent NO_2 levels. Riyadh experienced the most significant decrease in NO_2 after 2017, with an average reduction of 28.36% in the NO_2 tropospheric column during the 2017-2020 period compared to 2005-2008, a trend that not mirrored in the CAMS global anthropogenic emission inventory (*Figures S7*). Khartoum and Kuwait experienced an increase in the CH_2O tropospheric column average from the period 2005-2008 to 2017-2020, with rises of 11.09% and 12.17%, respectively. In contrast, Riyadh maintained nearly consistent CH_2O levels in the 2017-2020 period compared to 2005-2008, while Cairo exhibited a decreasing trend. Regarding the ozone production chemical regime, all cities maintained their previous chemical regimes, with Khartoum having a NO_x-limited regime during the summer and a transition during the rest of the year, Kuwait having a VOC-limited regime throughout the year, and Riyadh and Cairo having the same VOC-limited regime but nearing transition during the summer.

Overall, during the summer, Madrid transitioned from a VOC-limited regime to a near-transition regime, Lahore remained in the transition regime, and Delhi remained in the transition regime. Phoenix evolved from VOC-limited to nearly NO_x-limited, Los Angeles evolved to a transitional regime, and Baghdad and Tehran remained VOC-limited. Kuwait, Riyadh, and Cairo remained VOC-limited, while Khartoum remained NO_x-limited (2005-2020).

The factors behind the shifts in NO_2 and CH_2O levels in countries with emission controls, such as the U.S., Spain, China, and India, which include emission reduction strategies for industries and transport, resulting in NO_2 decline. However, VOCs showed minimal reductions, with some cities experiencing an increase. Specifically, Tehran, Baghdad, and Lahore in Asia, alongside Cairo in Africa, faced NO_2 emission increases due to economic growth and vehicle surges [54, 55, 60, 61]. Concurrently, a rise in VOCs has been attributed to increased energy consumption and solvent utilization [61].

Figure 3 shows TROPOMI's NO_2 and CH_2O columns between 2019-2022, reflecting increasing FNR variations, particularly in larger and more populous cities. A decrease in FNR correlates with increased population and aridity, pointing to a shift towards VOC-limited regimes. In addition, although cities were classified based on aridity index, *Figure S2* shows the remarkable diversity in local climate zones and land use within cities that share similar aridity indices. As shown in *Figure 4,* the diversity in urban landscapes

implies that even within a single city, there may be different 'micro-regimes' of ozone production. This variation is influenced by factors such as local industrial emissions, traffic, and the presence of green spaces, all of which affect ozone precursor levels such as NO_2 and VOCs. The study of micro-regimes within city boundaries necessitates high-resolution and accurate emissions, surface measurements of ozone concentration and precursors, and chemical transport models to investigate the diurnal change and transport of ozone and its precursors inside and outside city boundaries. Since polar orbiting satellites such as TROPOMI and OMI only pass in the early afternoon, they provide valuable insight into ozone production at the peak of photochemistry, but their coarse resolution and limited observation time make them only suitable for macro regime studies like this one, which only considers the average of ozone precursors within city boundaries. This could be a topic for local studies that use chemical transport models and higher-resolution geostationary satellites in the near future.

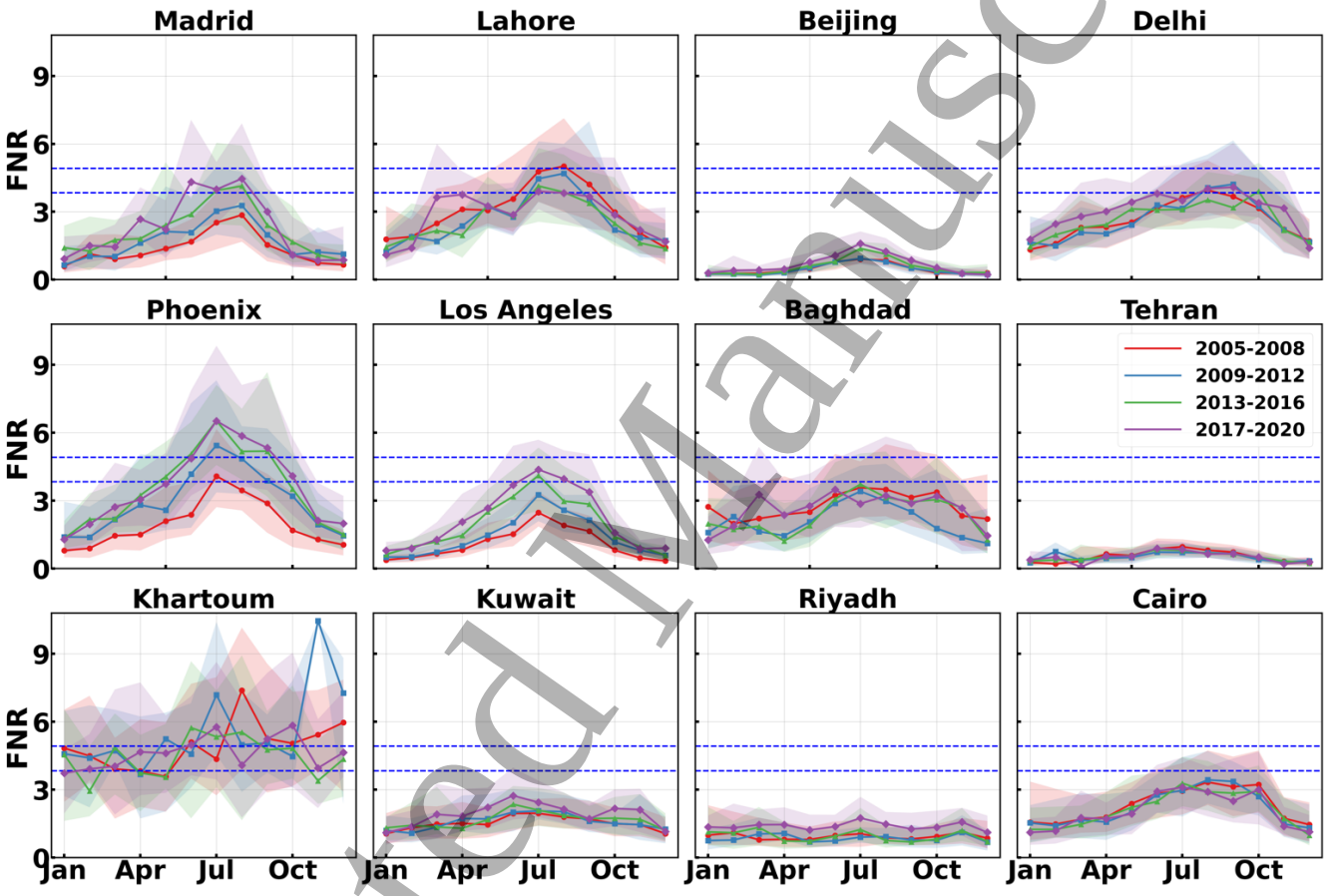

***Figure 2*. Seasonal variation of OMI tropospheric FNRs for 2005-2020 over semi-arid (first row), arid (second row), and hyper-arid (third row) cities. Solid lines indicate the median of all daily FNR values for 2005-2008 (red), 2009-2012 (blue), 2013-2016 (green), and 2017-2020 (purple). The shaded areas represent the interquartile ranges, highlighting the 25th to 75th percentiles of the FNRs.**

3.2 The impact of COVID 19 lockdowns on FNR

Using 2019 as a reference year and assuming no effect from COVID-19 emission fluctuations, all semi-arid cities, except Madrid, can be classified as transitional during the summer. The pandemic lockdowns primarily affected anthropogenic ozone precursors, specifically NO_x [59-62]. This is also consistent with a statistically significant ($p < 0.05$) decrease in TROPOMI tropospheric NO_2 columns, particularly during

spring and summer 2020. Among semi-arid cities, Lahore and Beijing showed a shift towards higher FNR values indicating a NO_x-limited regime during the summer, whereas Madrid and Delhi shifted to a transition regime. The inspection of *Figures S9* and *S10* reveals a general decline in NO_2 levels across these urban areas during the pandemic. Phoenix and Los Angeles, both arid cities, mirrored the increase in the FNR pattern, but Tehran and Baghdad did not exhibit significant NO_2 reductions in the summer and only Baghdad experienced NO_2 reduction during spring. As a result, the chemical regime during summer in Phoenix was NO_x-limited, in Los Angeles near transition, and Baghdad and Tehran remained in a VOC-limited regime. In hyper-arid cities, lower variations in NO_2 and consequently FNR were observed. These observations align with the CAMS global inventory, which indicates a substantial drop in NO_2 across eastern China, North America, Africa, and Europe during COVID-19 times [62]. Furthermore, despite a decrease in NO_x emissions as a result of lockdown measures, higher surface ozone concentrations were recorded in cities such as Madrid [63, 64], Beijing [65, 66], Delhi [67, 68], Los Angeles [69], Baghdad [70], and Tehran [71] especially during the COVID-19 lockdown in spring 2020. This paradox aligns with the changes in the FNR values and suggests that, in VOC-limited regimes, a reduction in NO_x may paradoxically escalate ozone production. In scenarios where NO_x levels are initially high, NO_x tends to sequester proxy radicals, leading to the formation of more NO_2 and, conversely, less ozone. However, when NO_x concentrations are reduced, chemical equilibrium is disrupted, favoring increased ozone generation from available VOCs.

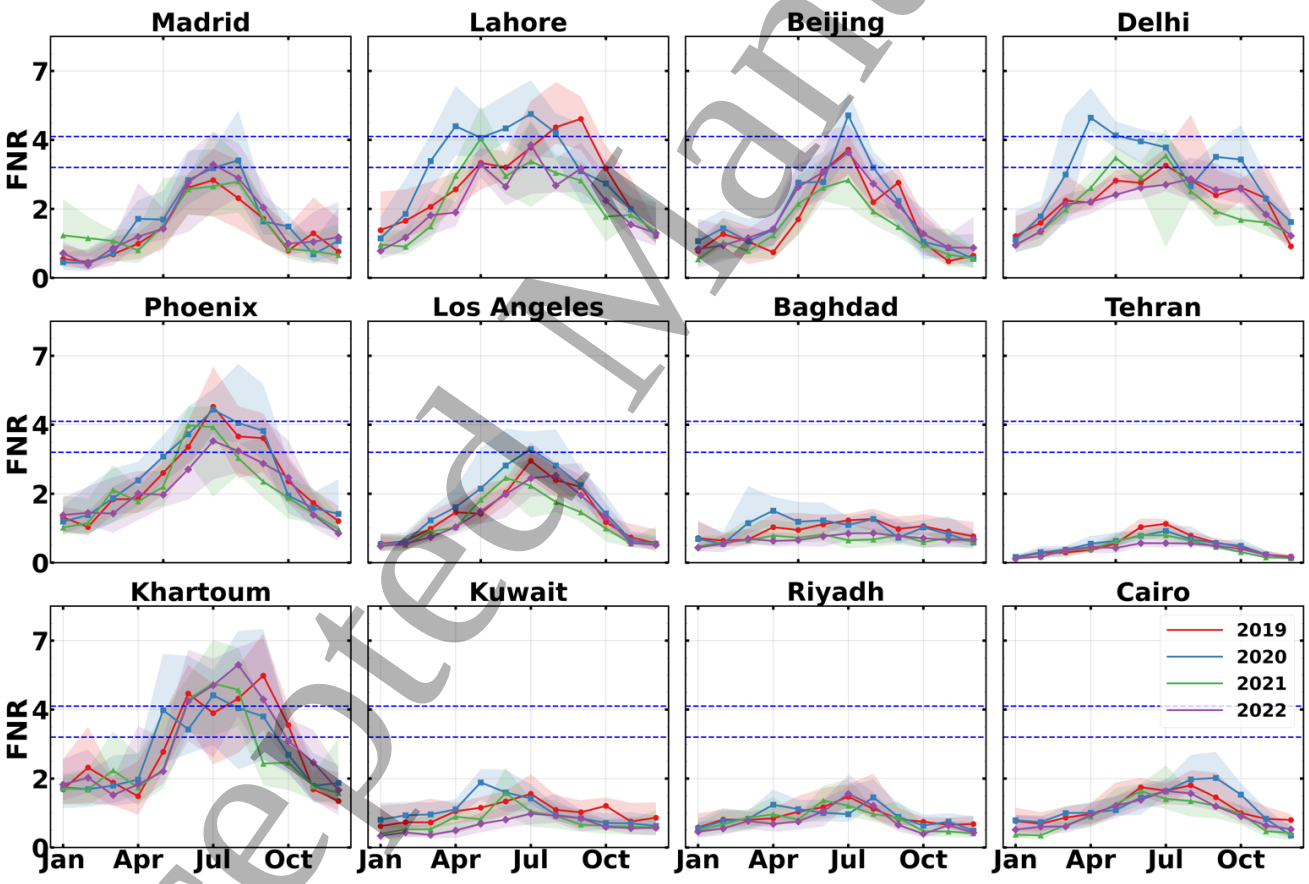

Figure 3. **Seasonal variation of TROPOMI tropospheric FNRs for 2019-2022 over semi-arid (first row), arid (second row), and hyper-arid (third row) cities. Solid lines indicate the median of all daily FNR values for 2019 (red), 2020 (blue), 2021 (green), and 2022 (purple). The shaded areas represent the interquartile ranges, highlighting the 25th to 75th percentiles of the FNRs.**

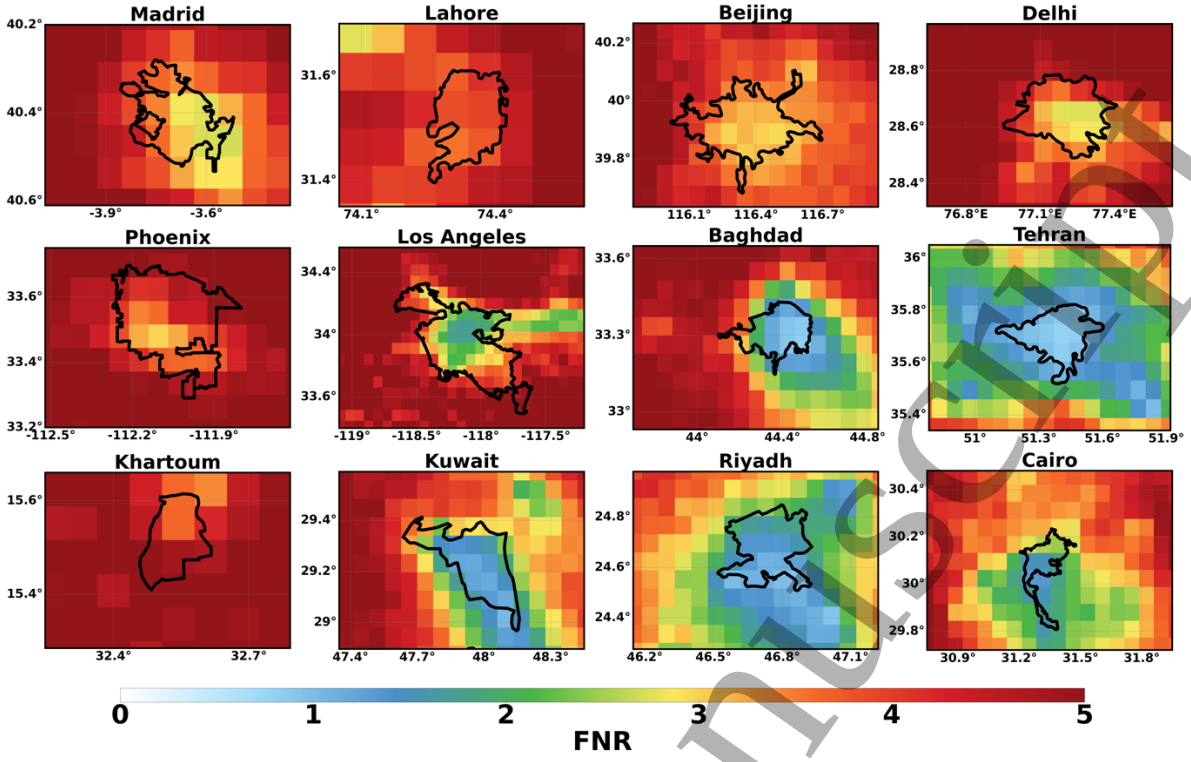

***Figure 4*. Spatial distribution of averaged daily TROPOMI tropospheric FNRs for 2019 to 2022 over semi-arid (first row), arid (second row), and hyper-arid (third row) cities. City boundaries are delineated with solid black lines.**

3.3 Relative dependence of FNR on meteorological parameters

The seasonality of ozone production is now compared to variations in meteorological parameters during the summer and winter. Beginning with temperature (*Figures S11*), hyper-arid and arid cities typically have higher summer temperatures than semi-arid cities, which increases energy demand for cooling [72, 73]. Conversely, their winter temperatures are not as low as those in the semi-arid regions. According to *Figure S12*, which shows the difference between all summer and winter day FNR values, Tehran, Baghdad, Riyadh, and Cairo showed the least seasonal change in FNR values.

Figure 5-A presents a comprehensive analysis of the daily FNR values across semi-arid, arid, and hyper-arid cities, revealing distinct seasonal variations. There is a clear distinction between the three aridity classes, whereas in the winter, the FNR primarily reflects a VOC-limited regime. Winter is distinguished by lower biogenic VOC emissions, less solar radiation, and, in some cases, higher NO_2 emissions, all of which are especially relevant in arid and semi-arid regions. This seasonality highlights the nonlinear relationship between the FNR indicator and temperature, further complicating the relationship between FNR and temperature across different aridity categories. We use the MI metric to gain insights into these nonlinear dependencies.

As shown in *Figure 5-B*, the MI scores for FNR's relationship with temperature were high in arid regions during the summer season, indicating a stronger dependency between FNR and temperature in ozone production under these conditions. This suggests that, as the temperature increases, the relationship between formaldehyde and NO_2 becomes a significant predictor of summer ozone levels in arid regions. In contrast, the hyper-arid and semi-arid regions showed lower MI scores for temperature during summer, indicating a less pronounced dependence of FNR on temperature in these regions. The MIs for winter

across all regions are significantly lower or zero, implying that the influence of temperature on FNR is less relevant during colder months, or that other factors may be more influential during this season. Regarding relative humidity, the MI scores were negligible across all regions and seasons, reinforcing that relative humidity does not appear to play a significant role in the relationship between FNR and ozone production. This indicates that the mechanisms controlling ozone production in these regions are less sensitive to changes in humidity, or that the influence of humidity on ozone production is not directly related to FNR levels.

The differences in MI scores between arid and hyper-arid regions, particularly during summer, can provide valuable insights into the meteorological and chemical processes that affect ozone production. These findings suggest that arid regions may require more attention to ambient temperature when modeling ozone production as temperature seems to have a stronger influence in these areas, potentially due to the specific regional climate or chemical conditions that amplify the nonlinear interactions between temperature and FNR.

Looking ahead, projections under the RCP 8.5 scenario anticipate a significant drying trend across North Africa and parts of the Middle East, with substantial reductions in precipitation expected in populated areas of the U.S., Europe, and China by mid-century [74]. These changes indicate that an increasing proportion of the world's population will reside in drier lands, a shift that will further redefine urban classifications into arid zones. Given this backdrop and the demonstrated nonlinearity of ozone production with respect to meteorological and chemical factors, there is an imperative to delve deeper into the drivers of ozone production in these drying regions. A holistic approach that combines surface measurements, chemical transport, and climate modeling with high-resolution satellite retrievals is necessary to discern the relative contributions of varying drivers to ozone production within these regions.

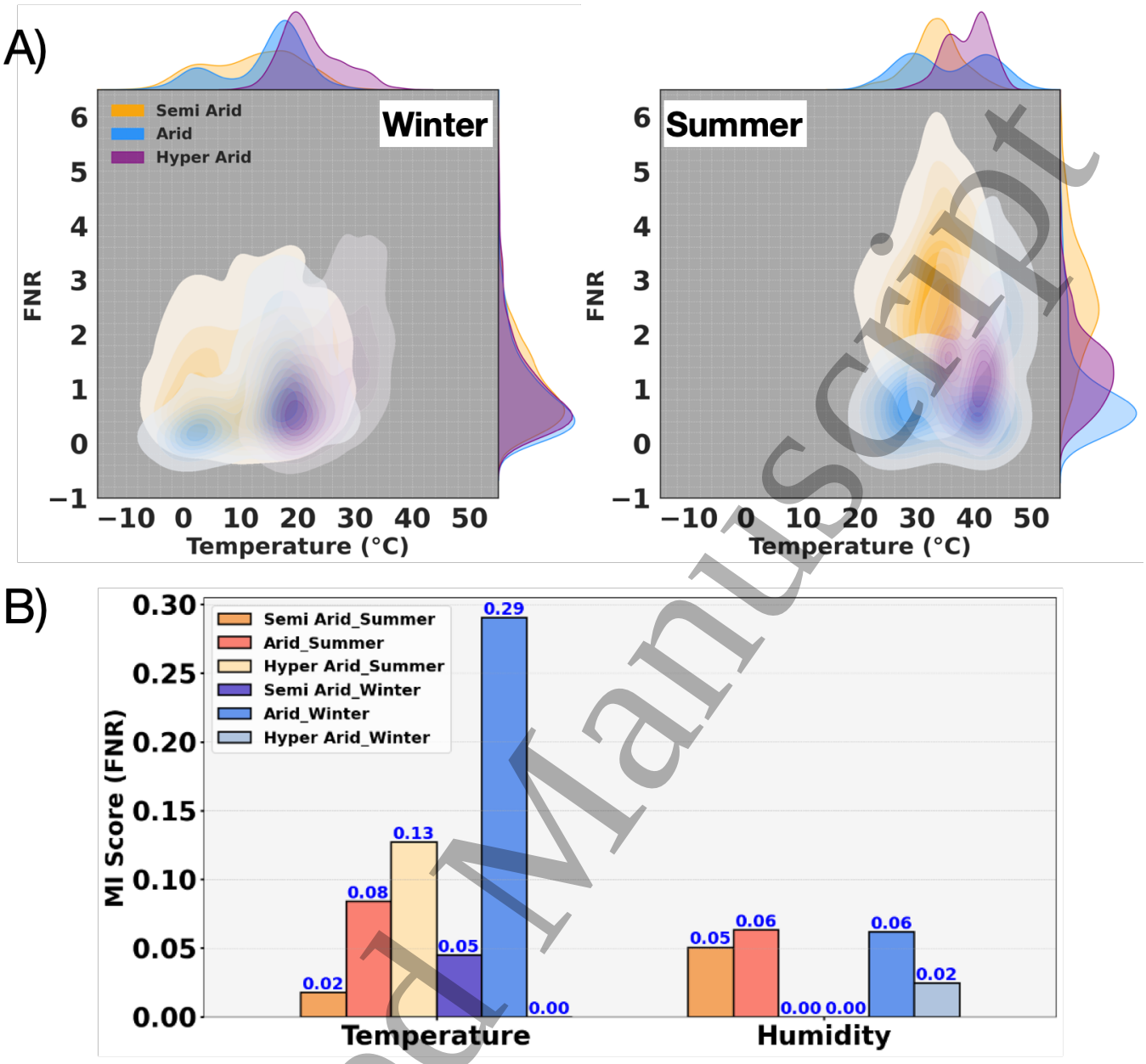

Figure 5. **A) TROPOMI tropospheric FNRs and temperature joint distribution for summer (JJA) and winter (DJF) for years 2019-2022 (the marginal probability distribution functions (pdfs) on vertical axis corresponding to pdfs of FNR in different aridity class and horizontal axis corresponds to pdfs of temperature (yellow: semi-arid, blue: arid and purple: hyper-arid). B) Mutual information (MI) score of the dependence of FNR on temperature and relative humidity.**

4. Conclusion

This study aims to draw attention to the state of tropospheric ozone production in arid cities worldwide. We classified these cities according to their population and level of aridity using the most recent and widely used index for aridity. Tropospheric NO_2 and CH_2O columns of TROPOMI and OMI satellite instruments were used to quantify the decadal and current levels of ozone production precursors by characterizing the chemical regime in each city using a spaced-based FNR, which is representative of the

relative availability of total organic reactivity to hydroxyl radicals and NO_x. The temporal trend of ozone production in recent decades is consistent with the reported economic growth and emission control strategies of different countries. Cities located in countries with established emission control plans, such as Madrid, Los Angeles, Phoenix, and Beijing, which are located in semi-arid and arid regions, appear to experience a reduction in the tropospheric NO_2 column. However, for cities in the Middle East and Africa like Tehran, Baghdad, and Cairo, which are mostly in arid and hyper-arid climates, rapid economic growth, especially in the energy sector, and an apparent lack of emission control plans appears to lead to higher NO_2 levels in these regions. In addition, despite the reduction in NO_2 levels in some cities, the temporal trend of CH_2O showed an increase in most cities, which warrants more attention from policymaking standpoint.

To our knowledge, this is one of the few studies that has investigated ozone production in several representative cities with the same aridity level. The application of space-based ozone production indicators in previous studies was limited to a region or continent, and the recommended thresholds for defining NO_x- and VOC-limited regimes were based on surface measurement in the U.S., which were not applied globally as we have in this work. While this study shows good agreement with previous literature, additional long-term observations of surface ozone and its precursors as well as reliable high-resolution emission inventories are required for a more detailed assessment of ozone production. Finally, the NO_x/VOC-limited regimes in semi-arid, arid, and hyper-arid regions showed a robust nonlinear relationship with temperature and relative humidity; however, there was a higher dependence of FNR on temperature in arid regions.

With global aridity expected to expand to new regions, we highlight the importance of studying these relationships in arid cities to provide insights into the potential response of ozone production to increasing urbanization in a changing climate.

Data availability statement

Data supporting this study's findings can be made available by the authors upon request.

Acknowledgements

Funding for this work was provided by the Arizona Board of Regents (ABOR) Regent's Grant from the Technology and Research Initiative Fund (TRIF). We acknowledge Benjamin Gaubert (NCAR/ACOM) and Kazuyuki Miyazaki (NASA/JPL) for their helpful suggestions.

Conflict of interest

The authors declare that they have no conflict of interest.

References

[1] (IPCC), "Climate Change 2013 – The Physical Science Basis," I. P. o. C. Change and Eds., ed: Cambridge University Press, 2014.
[2] G. Del Barrio, M. E. R. A. Sanjuán, J. Martínez-Valderrama, J. Puigdefábregas, and "World Atlas of Desertification Third Edition," ed, 2018.
[3] UNEP, "World atlas of desertification. Second edition," ed, 1997.
[4] R. J. Zomer, J. Xu, and A. Trabucco, "Version 3 of the global aridity index and potential evapotranspiration database," *Scientific Data,* vol. 9, no. 1, p. 409, 2022.
[5] U. Nations, "The World's Cities in 2018—Data Booklet," vol. a, ed, 2018.

[6] U. Environment, "GLOBAL ENVIRONMENT OUTLOOK GEO-6 HEALTHY PLANET, HEALTHY PEOPLE," ed: Cambridge University Press, 2019, pp. iii-v.

[7] M. Svoboda and B. Fuchs, "Handbook of drought indicators and indices," *Drought and water crises: Integrating science, management, and policy,* pp. 155-208, 2016.

[8] K. Trenberth, J. Overpeck, and S. Solomon, "Exploring drought and its implications for the future," ed: Wiley Online Library, 2004.

[9] A. M. Thomson *et al.*, "RCP4. 5: a pathway for stabilization of radiative forcing by 2100," *Climatic change,* vol. 109, pp. 77-94, 2011.

[10] K. Riahi *et al.*, "RCP 8.5—A scenario of comparatively high greenhouse gas emissions," *Climatic change,* vol. 109, pp. 33-57, 2011.

[11] S. Osipov *et al.*, "Severe atmospheric pollution in the Middle East is attributable to anthropogenic sources," *Communications Earth & Environment,* vol. 3, no. 1, p. 203, 2022.

[12] S. E. Pusede, A. L. Steiner, and R. C. Cohen, "Temperature and recent trends in the chemistry of continental surface ozone," *Chemical reviews,* vol. 115, no. 10, pp. 3898-3918, 2015.

[13] S. Sillman and P. J. Samson, "Impact of temperature on oxidant photochemistry in urban, polluted rural and remote environments," *Journal of Geophysical Research: Atmospheres,* vol. 100, no. D6, pp. 11497-11508, 1995.

[14] M. Lin *et al.*, "Vegetation feedbacks during drought exacerbate ozone air pollution extremes in Europe," *Nature Climate Change,* vol. 10, no. 5, pp. 444-451, 2020.

[15] N. Otero, H. W. Rust, and T. Butler, "Temperature dependence of tropospheric ozone under NOx reductions over Germany," *Atmospheric Environment,* vol. 253, p. 118334, 2021.

[16] S. Pugliese, J. Murphy, J. Geddes, and J. Wang, "The impacts of precursor reduction and meteorology on ground-level ozone in the Greater Toronto Area," *Atmospheric Chemistry and Physics,* vol. 14, no. 15, pp. 8197-8207, 2014.

[17] S. Pusede and R. Cohen, "On the observed response of ozone to NO x and VOC reactivity reductions in San Joaquin Valley California 1995–present," *Atmospheric Chemistry and Physics,* vol. 12, no. 18, pp. 8323-8339, 2012.

[18] S. Pusede *et al.*, "On the temperature dependence of organic reactivity, nitrogen oxides, ozone production, and the impact of emission controls in San Joaquin Valley, California," *Atmospheric Chemistry and Physics,* vol. 14, no. 7, pp. 3373-3395, 2014.

[19] M. Xie *et al.*, "Application of photochemical indicators to evaluate ozone nonlinear chemistry and pollution control countermeasure in China," *Atmospheric environment,* vol. 99, pp. 466-473, 2014.

[20] P. Wang, S. Zhu, M. Vrekoussis, G. P. Brasseur, S. Wang, and H. Zhang, "Is atmospheric oxidation capacity better in indicating tropospheric O3 formation?," *Frontiers of Environmental Science & Engineering,* vol. 16, no. 5, p. 65, 2022.

[21] C. Liu and K. Shi, "A review on methodology in O3-NOx-VOC sensitivity study," *Environmental Pollution,* vol. 291, p. 118249, 2021.

[22] J. L. Pearce, J. Beringer, N. Nicholls, R. J. Hyndman, and N. J. Tapper, "Quantifying the influence of local meteorology on air quality using generalized additive models," *Atmospheric Environment,* vol. 45, no. 6, pp. 1328-1336, 2011.

[23] C. Hu *et al.*, "Understanding the impact of meteorology on ozone in 334 cities of China," *Atmospheric Environment,* vol. 248, p. 118221, 2021.

[24] B. Vogel, N. Riemer, H. Vogel, and F. Fiedler, "Findings on NO y as an indicator for ozone sensitivity based on different numerical simulations," *Journal of Geophysical Research: Atmospheres,* vol. 104, no. D3, pp. 3605-3620, 1999.

[25] X. Lu, L. Zhang, and L. Shen, "Meteorology and climate influences on tropospheric ozone: a review of natural sources, chemistry, and transport patterns," *Current Pollution Reports,* vol. 5, pp. 238-260, 2019.

[26] S. Sillman, "The relation between ozone, NOx and hydrocarbons in urban and polluted rural environments," *Atmospheric Environment,* vol. 33, no. 12, pp. 1821-1845, 1999.

[27] A. H. Souri *et al.*, "Characterization of errors in satellite-based HCHO⁄NO 2 tropospheric column ratios with respect to chemistry, column-to-PBL translation, spatial representation, and retrieval uncertainties," *Atmospheric Chemistry and Physics,* vol. 23, no. 3, pp. 1963-1986, 2023.

[28] S.-W. Kim *et al.*, "Impact of high-resolution a priori profiles on satellite-based formaldehyde retrievals," *Atmospheric Chemistry and Physics,* vol. 18, no. 10, pp. 7639-7655, 2018.

[29] C. Li *et al.*, "Investigating the vertical distribution patterns of urban air pollution based on unmanned aerial vehicle gradient monitoring," *Sustainable Cities and Society,* vol. 86, p. 104144, 2022.

[30] E. A. Kort and K. McKain, "Aircraft vertical profile measurements for evaluation of satellite retrievals of long-lived trace gases," in *Field Measurements for Passive Environmental Remote Sensing*: Elsevier, 2023, pp. 235-244.

[31] R. V. Martin, A. M. Fiore, and A. Van Donkelaar, "Space-based diagnosis of surface ozone sensitivity to anthropogenic emissions," *Geophysical Research Letters,* vol. 31, no. 6, 2004.

[32] B. N. Duncan *et al.*, "Application of OMI observations to a space-based indicator of NOx and VOC controls on surface ozone formation," *Atmospheric Environment,* vol. 44, no. 18, pp. 2213-2223, 2010.

[33] X. Jin, A. Fiore, K. F. Boersma, I. D. Smedt, and L. Valin, "Inferring changes in summertime surface Ozone–NO x–VOC chemistry over US urban areas from two decades of satellite and ground-based observations," *Environmental science & technology,* vol. 54, no. 11, pp. 6518-6529, 2020.

[34] ESRI. "World Urban Areas." https://hub.arcgis.com/datasets/esri::world-urban-areas (accessed 10 October, 2023.

[35] M. Demuzere *et al.*, "A global map of local climate zones to support earth system modelling and urban-scale environmental science," *Earth Syst. Sci. Data,* vol. 14, no. 8, pp. 3835-3873, 2022, doi: 10.5194/essd-14-3835-2022.

[36] J. J. M. Acdan, R. B. Pierce, A. F. Dickens, Z. Adelman, and T. Nergui, "Examining TROPOMI formaldehyde to nitrogen dioxide ratios in the Lake Michigan region: implications for ozone exceedances," *Atmos. Chem. Phys.,* vol. 23, no. 14, pp. 7867-7885, 2023, doi: 10.5194/acp-23-7867-2023.

[37] M. Tao *et al.*, "Investigating changes in ozone formation chemistry during summertime pollution events over the Northeastern United States," *Environmental Science & Technology,* vol. 56, no. 22, pp. 15312-15327, 2022.

[38] A. Ludewig *et al.*, "In-flight calibration results of the TROPOMI payload on board the Sentinel-5 Precursor satellite," *Atmospheric Measurement Techniques,* vol. 13, no. 7, pp. 3561-3580, 2020.

[39] J. Van Geffen *et al.*, "S5P TROPOMI NO 2 slant column retrieval: Method, stability, uncertainties and comparisons with OMI," *Atmospheric Measurement Techniques,* vol. 13, no. 3, pp. 1315-1335, 2020.

[40] I. De Smedt, F. Romahn, and K.-U. Eichmann, "S5P Mission Performance Centre Formaldehyde [L2__HCHO___] Readme," 2023. [Online]. Available: https://sentinels.copernicus.eu/documents/247904/3541451/ Sentinel-5P-Formaldehyde-Readme.pdf.

[41] H. J. Eskes and K.-U. Eichmann, "S5P Mission Performance Centre Nitrogen Dioxide [L2__NO2___] Readme," 2023. [Online]. Available: https://sentinel.esa.int/documents/247904/3541451/Sentinel-5P-Nitrogen-Dioxide-Level-2-Product-Readme-File.

[42] K. Boersma *et al.*, "Near-real time retrieval of tropospheric NO 2 from OMI," *Atmospheric Chemistry and Physics,* vol. 7, no. 8, pp. 2103-2118, 2007.

[43] P. F. Levelt *et al.*, "The ozone monitoring instrument," *IEEE Transactions on geoscience and remote sensing,* vol. 44, no. 5, pp. 1093-1101, 2006.

[44] L. N. Lamsal *et al.*, "Ozone Monitoring Instrument (OMI) Aura nitrogen dioxide standard product version 4.0 with improved surface and cloud treatments," *Atmospheric Measurement Techniques,* vol. 14, no. 1, pp. 455-479, 2021.

[45] I. De Smedt *et al.*, "QA4ECV HCHO tropospheric column data from OMI (Version 1.1)[Data set]," *Royal Netherlands Meteorological Institute (KNMI), doi,* vol. 10, p. 71021031, 2017.

[46] A. Lorente *et al.*, "Structural uncertainty in air mass factor calculation for NO 2 and HCHO satellite retrievals," *Atmospheric Measurement Techniques,* vol. 10, no. 3, pp. 759-782, 2017.

[47] C. C. C. Service, "ERA5: Fifth generation of ECMWF atmospheric reanalyses of the global climate," *Copernicus Climate Change Service Climate Data Store (CDS),* vol. 15, no. 2, p. 2020, 2017.

[48] M. G. Lawrence, "The relationship between relative humidity and the dewpoint temperature in moist air: A simple conversion and applications," *Bulletin of the American Meteorological Society,* vol. 86, no. 2, pp. 225-234, 2005.

[49] A. Inness *et al.*, "The CAMS reanalysis of atmospheric composition," *Atmospheric Chemistry and Physics,* vol. 19, no. 6, pp. 3515-3556, 2019.

[50] J. B. Kinney and G. S. Atwal, "Equitability, mutual information, and the maximal information coefficient," *Proceedings of the National Academy of Sciences,* vol. 111, no. 9, pp. 3354-3359, 2014.

[51] P. Laarne, M. A. Zaidan, and T. Nieminen, "ennemi: Non-linear correlation detection with mutual information," *SoftwareX,* vol. 14, p. 100686, 2021.

[52] A. Kraskov, H. Stögbauer, and P. Grassberger, "Estimating mutual information," *Physical review E,* vol. 69, no. 6, p. 066138, 2004.

[53] C. E. Shannon, "A mathematical theory of communication," *The Bell system technical journal,* vol. 27, no. 3, pp. 379-423, 1948.

[54] B. N. Duncan *et al.*, "A space-based, high-resolution view of notable changes in urban NOx pollution around the world (2005–2014)," *Journal of Geophysical Research: Atmospheres,* vol. 121, no. 2, pp. 976-996, 2016.

[55] M. Bauwens, B. Verreyken, T. Stavrakou, J. Müller, and I. De Smedt, "Spaceborne evidence for significant anthropogenic VOC trends in Asian cities over 2005–2019," *Environmental Research Letters,* vol. 17, no. 1, p. 015008, 2022.

[56] J. Ren, Y. Hao, M. Simayi, Y. Shi, and S. Xie, "Spatiotemporal variation of surface ozone and its causes in Beijing, China since 2014," *Atmospheric Environment,* vol. 260, p. 118556, 2021.

[57] A. Soulie *et al.*, "Global Anthropogenic Emissions (CAMS-GLOB-ANT) for the Copernicus Atmosphere Monitoring Service Simulations of Air Quality Forecasts and Reanalyses," *Earth Syst. Sci. Data Discuss.,* vol. 2023, pp. 1-45, 2023, doi: 10.5194/essd-2023-306.

[58] F. Shen *et al.*, "Disentangling drivers of air pollutant and health risk changes during the COVID-19 lockdown in China," *npj Climate and Atmospheric Science,* vol. 5, no. 1, p. 54, 2022.
[59] C. M. Nussbaumer and R. C. Cohen, "The role of temperature and NO x in ozone trends in the Los Angeles Basin," *Environmental Science & Technology,* vol. 54, no. 24, pp. 15652-15659, 2020.
[60] S. Torbatian, A. Hoshyaripour, H. Shahbazi, and V. Hosseini, "Air pollution trends in Tehran and their anthropogenic drivers," *Atmospheric Pollution Research,* vol. 11, no. 3, pp. 429-442, 2020.
[61] M. Al-Mutairi, N. Al-Otaibi, A. Saber, H. Abdel Basset, and M. Morsy, "Climatological Study of Air Pollutant Emissions in Saudi Arabia," *Atmosphere,* vol. 14, no. 4, p. 729, 2023.
[62] T. Doumbia *et al.*, "Changes in global air pollutant emissions during the COVID-19 pandemic: a dataset for atmospheric modeling," *Earth Syst. Sci. Data,* vol. 13, no. 8, pp. 4191-4206, 2021, doi: 10.5194/essd-13-4191-2021.
[63] M. A. Betancourt-Odio, C. Martínez-de-Ibarreta, S. Budría-Rodríguez, and E. Wirth, "Local analysis of air quality changes in the community of Madrid before and during the COVID-19 induced lockdown," *Atmosphere,* vol. 12, no. 6, p. 659, 2021.
[64] Q. Wang and S. Li, "Nonlinear impact of COVID-19 on pollutions–Evidence from Wuhan, New York, Milan, Madrid, bandra, London, tokyo and Mexico city," *Sustainable Cities and Society,* vol. 65, p. 102629, 2021.
[65] T. Wang, L. Xue, Z. Feng, J. Dai, Y. Zhang, and Y. Tan, "Ground-level ozone pollution in China: a synthesis of recent findings on influencing factors and impacts," *Environmental Research Letters,* vol. 17, no. 6, p. 063003, 2022.
[66] W. Wang *et al.*, "Long-term trend of ozone pollution in China during 2014–2020: Distinct seasonal and spatial characteristics and ozone sensitivity," *Atmospheric Chemistry and Physics,* vol. 22, no. 13, pp. 8935-8949, 2022.
[67] L. R. Crilley, Y. E. Iranpour, and C. J. Young, "Importance of meteorology and chemistry in determining air pollutant levels during COVID-19 lockdown in Indian cities," *Environmental Science: Processes & Impacts,* vol. 23, no. 11, pp. 1718-1728, 2021.
[68] S. Das *et al.*, "Trends in summer-time tropospheric ozone during covid-19 lockdown in Indian cities might forecast a higher future risk," *Atmosphere,* vol. 13, no. 7, p. 1115, 2022.
[69] I. Leifer, C. Melton, D. R. Blake, S. Meinardi, and M. Kleinman, "Air quality trends for the ports of Los Angeles and Long Beach spanning the covid19 crisis: Part 1. Oxidant pollutants," *Atmospheric Environment,* vol. 312, p. 119949, 2023.
[70] B. M. Hashim, S. K. Al-Naseri, A. Al-Maliki, and N. Al-Ansari, "Impact of COVID-19 lockdown on NO2, O3, PM2. 5 and PM10 concentrations and assessing air quality changes in Baghdad, Iraq," *Science of the Total Environment,* vol. 754, p. 141978, 2021.
[71] M. Bagherinia, S. Bodaghpour, N. Karimi, F. Ghasempour, M. Bilal, and A. Mhawish, "Spatio-temporal air quality assessment in Tehran, Iran, during the COVID-19 lockdown periods," *Geocarto International,* p. 2169374, 2023.
[72] S. M. Wahba, B. A. Kamel, K. M. Nassar, and A. S. Abdelsalam, "Effectiveness of green roofs and green walls on energy consumption and indoor comfort in arid climates," *Civil Engineering Journal,* vol. 4, no. 10, pp. 2284-2295, 2018.
[73] A. Rey-Pommier *et al.*, "Quantifying NOx emissions in Egypt using TROPOMI observations," *Atmos. Chem. Phys.,* vol. 22, no. 17, pp. 11505-11527, 2022, doi: 10.5194/acp-22-11505-2022.
[74] M. Lickley and S. Solomon, "Drivers, timing and some impacts of global aridity change," *Environmental Research Letters,* vol. 13, no. 10, p. 104010, 2018.